Miocene to Pliocene development of surface and sub-surface temperatures in the Benguela Current System

Florian Rommerskirchen*

Marum – Center for Marine Environmental Sciences, University of Bremen, P.O. Box 330 440, D-28334 Bremen, Germany. Phone: +49 421 218 – 65527. E-mail address: rommerskirchen@uni-bremen.de.

Tegan Condon

Marum – Center for Marine Environmental Sciences, University of Bremen, P.O. Box 330 440, D-28334 Bremen, Germany.
Present address: Department of Earth & Planetary Sciences, Havard University, 20 Oxford Street, Cambridge, MA 02138 USA. E-mail address: tegdon@gmail.com.

Gesine Mollenhauer

Alfred Wegener Institute for Polar and Marine Research, D-27570 Bremerhaven, Germany. E-mail address: gesine.mollenhauer@awi.de.

Lydie Dupont

Marum – Center for Marine Environmental Sciences, University of Bremen, P.O. Box 330 440, D-28334 Bremen, Germany. E-mail address: dupont@uni-bremen.de.

Enno Schefuß

Marum – Center for Marine Environmental Sciences, University of Bremen, P.O. Box 330 440, D-28334 Bremen, Germany. E-mail address: schefuss@uni-bremen.de.

*) Corresponding author

Abstract

The initiation of Benguela upwelling has been dated in the late Miocene, but estimates of its sea surface temperature evolution are not available. This study presents data from ODP Site 1085 recovered from the southern Cape Basin. Samples of the Middle Miocene to Pliocene were analyzed for alkenone based ($U^{K'}_{37}$, SST_{UK}) and glycerol dialkyl glycerol tetraether (GDGT) based (TEX_{86}, $Temp_{TEX}$) water temperature proxies. In concordance with global cooling during the Miocene, SST_{UK} and $Temp_{TEX}$ exhibit a decline of about 8 and 16°C, respectively. The temperature trends suggest an inflow of cold Antarctic waters triggered by Antarctic ice sheet expansion and intensification of Southern Hemisphere south-easterly winds. A temperature offset between both proxies developed with the onset of upwelling, which can be explained by differences in habitat: alkenone-producing phytoplankton live in the euphotic zone and record sea-surface temperatures, while GDGT-producing Thaumarchaeota were displaced to colder sub-surface waters in upwelling-influenced areas and record sub-surface water temperatures. We suggest that variations in sub-surface water temperatures were driven by advection of cold Antarctic waters and thermocline adjustments due to changes in North Atlantic deepwater formation. Decline in surface temperatures, increased offset between temperature proxies and increase in primary productivity suggest establishment of Benguela upwelling at 10 Ma. During the Messinian Salinity Crisis, between 7 and 5 Ma, surface and sub-surface temperature estimates became similar, likely due to a strong reduction in Atlantic overturning circulation, while high total organic carbon (TOC) contents suggest a "biogenic bloom". In the Pliocene the offset between the temperature estimates and the cooling trend re-established.

Keywords

ODP Site 1085, Miocene, Pliocene, SST, sub-surface temperature, Benguela, upwelling, GDGT, alkenone, UK'37, TEX86

1. Introduction

One of today's major coastal upwelling areas is located in the Southeast Atlantic Ocean within the Benguela Upwelling System (BUS). Upwelling of cold and nutrient-rich Antarctic sourced waters supports vast populations of phytoplankton, which are the basis for the World's richest fishing ground (productivity > 180 gC/m^2/year) [*Berger*, 1989; *Shannon and Nelson*, 1996; *Wefer et al.*, 1996; *Wefer et al.*, 1998]. It is believed that the BUS has originated in the early late Miocene [*Diester-Haass et al.*, 1990; *Robert et al.*, 2005; *Siesser*, 1980]. Generally, the Miocene epoch represents the transition from a relatively warm Eocene greenhouse climate to cooler, drier and less stable conditions, when fluctuating Antarctic ice-sheets permanently established [*Flower and Kennett*, 1994; *Zachos et al.*, 2001]. Major growth of East Antarctic ice-sheets after the middle Miocene climatic optimum (around 16 Ma) affected atmospheric and oceanographic circulation and led to the rapid cooling of mid- to high-latitudes, greater zonality and stronger surface ocean circulation due to enhanced deep water production [*Flower and Kennett*, 1994; *Zachos et al.*, 2001]. In response, wind-driven upwelling of cold and nutrient-rich waters occurred in distinct cells along the coast of Southwest Africa with locally slight delays [*Diester-Haass*, 1988; *Diester-Haass and Rothe*, 1987; *Siesser*, 1980]. Sedimentological data, clay mineral assemblages and abundance of specific fossil skeletons of microorganisms date the initiation of the BUS at approximately 9-10 Ma [*Diester-Haass et al.*, 1990; *Krammer et al.*, 2006; *Robert et al.*, 2005; *Siesser*, 1980]. Presumably, the initiation resulting in a decline of sea surface temperatures (SSTs) along the coast of Southwest Africa. However, no studies so far have covered the Miocene thermal development of the BUS. SST studies outside the Benguela system found SST decreases of over 3 to 10°C, depending on latitude [*Williams et al.*, 2005], and attributed these to the global cooling triggered by Miocene Antarctic ice-sheet expansion [*Billups and Schrag*, 2002; *Herbert and Schuffert*, 1998; *Kuhnert et al.*, 2009; *Lear et al.*, 2000; *Shevenell et al.*, 2004].

Due to lack of data, the ocean temperature development in conjunction with the initiation and development of upwelling during the intensification of the BUS is yet poorly understood.

Here we present ocean temperature data from the middle Miocene to Pliocene covering a time span of almost 11 Myr between 13.7 and 2.8 Ma. Our area of investigation is located in the Cape Basin in front of the South African Orange River. We use two different organic geochemical temperature proxies: the alkenone unsaturation index ($U^{K'}_{37}$, SST_{UK}) [*Brassell et al.*, 1986] and the TEX_{86} index using a ratio of glycerol dialkyl glycerol tetraethers (GDGTs) with different numbers of cyclopentane rings, the tetraether index ($Temp_{TEX}$) [*Schouten et al.*, 2002]. While it was originally assumed that both proxies reflect SST [*Schouten et al.*, 2002], differences between these two temperature proxies were found which potentially are related to differences in the habitat of the source organisms in specific oceanic areas [e.g. *Huguet et al.*, 2006; *Lee et al.*, 2008]. In this study, we aim to disentangle the additional information that can be obtained from applying two ocean temperature proxies and attempt to decipher sea water temperature and upwelling changes in conjunction with global oceanographic events.

2. Benguela Upwelling System and Hydrography of the Cape Basin

Today's surface water circulation in the Southeast Atlantic is dominated by the Benguela Current (BC), which flows northward along the southwest coast of Africa (Figure 1). It originates from the eastward directed cold South Atlantic Current, the northernmost front of the Antarctic Circumpolar Current (ACC), and the warm Agulhas Current (AgC) flowing from the Indian Ocean around the Cape of Good Hope where it retroflects (Figure 1) [*Peterson and Stramma*, 1991]. The BC divides into the Benguela Ocean Current (BOC) and Benguela Coastal Current (BCC) around 28°S on its northward flow. The BOC flows north-westward and crosses the Atlantic Ocean as the South Equatorial Current, while the

northward directed BCC encounters the southward directed warm Angola Current north of the Walvis Ridge at the Angola-Benguela Front [*Peterson and Stramma*, 1991].

The present Southeast Atlantic deep water circulation depends on interactions of the southward flowing relatively warm, highly-saline, oxygen-rich and nutrient-poor North Atlantic Deep Water (NADW) and the northward flowing relatively cold, oxygen-poor and nutrient-rich Antarctic deep water masses [*Berger and Wefer*, 1996b; *Broecker et al.*, 1985; *Reid*, 1989]. In the Cape Basin, NADW occurs between 2500 and 4000 m water depth sandwiched between the cold water masses of the Antarctic (Figure 1). The hydrography between approximately 2500 and 500 m water depth is generally characterized by Antarctic Intermediate Water (AAIW) and Upper Circumpolar Deep Water (UCDW) (Figure 1). South Atlantic surface waters down to approximately 400 m are warm and salty (15 to 23°C and 35.4 to 36.0 psu) compared to AAIW located underneath (6 to 16°C and 34.5 to 35.5 psu) [*Schneider et al.*, 2003], which leads to a strong permanent thermocline. Along the East Atlantic margin the cold thermocline waters extend to the bottom of the continental shelf and are uplifted to the surface in the upwelling cells along the African coast [*Andrews and Hutchings*, 1980].

Upwelling along the southwest African coast occurs in small upwelling cells in response to southeast trade wind-induced Ekman transport. Strongest perennial upwelling within the Cape Basin takes place in the northern part of the BUS (19 - 28°S) between Lüderitz and the Walvis Ridge and extends 130-230 km offshore (Figure 1, grey shaded areas) [*Shannon and Nelson*, 1996]. Less intense and smaller upwelling cells are located south of Lüderitz in the southern part of the BUS (28 - 34°S) [*Shannon and Nelson*, 1996]. Within these cells upwelling of cold and nutrient-rich Antarctic waters from 200 to 500 m water depth induces perennial high productivity [*Hart and Currie*, 1960; *Lutjeharms and Meeuwis*, 1987; *Lutjeharms and Stockton*, 1987]. Intensified southeast trade winds during austral summer

(December to April) lead to enhanced upwelling and upwelling filaments may extend up to 600 km offshore [*Lutjeharms and Stockton*, 1987; *Summerhayes et al.*, 1995]. Secondary upwelling may occur at a shelf-break thermal front sometimes extending 1300 km offshore [*Summerhayes et al.*, 1995].

3. Material and Methods

3.1. Study Area and Samples

We analyzed samples from Ocean Drilling Program (ODP) Hole 1085 A that was drilled in 1997 during ODP Leg 175 on the south-west African continental margin (core position: 29°22. 5'S, 13°59.4'E, 1713 m water depth; Figure 1; [*Wefer et al.*, 1998]). The site is situated in the Mid-Cape Basin south of the modern upwelling center. Today, the site is influenced by filaments of seasonal upwelling [*Lutjeharms and Stockton*, 1987]. Annual mean SSTs are around 17.9°C, while warmer temperatures occur during the austral summer (ca. 20.1°C, January to March) and colder during the austral winter (ca. 15.9°C, July to September) [*Locarnini et al.*, 2010]. Seasonal temperature changes have an impact down to a depth of ca. 125 m [*Locarnini et al.*, 2010]. A temperature depth profile of nearby GeoB Site 8337 indicates a surface mixed layer of 40 m water depth [*Lee et al.*, 2008]. In surface waters, concentrations of silica and phosphate as well as primary productivity are relatively low compared to the northern part of the upwelling area [*Berger et al.*, 2002; *Mollenhauer et al.*, 2002].

ODP Site 1085 is located approximately 300 km away from the river mouth of the perennial Orange River at the margin of today's river plume, which carries suspended terrigenous material. The shelf in this area is relatively wide (180 km) [*Shannon and Nelson*, 1996; *Wefer et al.*, 1998]. The Orange River discharges on average 0.02 $Gt.yr^{-1}$ organic

carbon [*Compton et al.*, 2009]. The sediment load is transported to the shelf and slope and distributed southward by near-shore south-flowing counter currents [*Bremner et al.*, 1990; *Summerhayes et al.*, 1995].

A high resolution age model based on oxygen isotope ratios ($\delta^{18}O$) of benthic foraminifera and X-ray fluorescence scanning (Fe and Ca) provides a detailed chronology for the late Miocene to early Pliocene (13.9 to 4.7 Ma) [*Vidal et al.*, 2002; *Westerhold et al.*, 2005]. Ages of Pliocene and Pleistocene samples were determined by using an age model based on biostratigraphic and paleomagnetic events [*Berger et al.*, 2002]. 66 samples of ca. 10 mL sediment were taken between 134 and 592 m composite depth dated from 2.8 to 13.7 Ma. For comparison three samples were selected from the late Pleistocene (14.8, 32.0, and 69.3 ka, cf. Table 1).

3.2. Analytical and Evaluation Methods

Before sampling at the IODP Core Repository in Bremen cores of ODP Leg 175 Site 1085 were stored at 4°C since their recovery. Sediment samples were freeze-dried and ground and homogenized by mortar and pestle. Total organic carbon (TOC) contents were determined by decarbonating a sediment aliquot of ca. 25 mg using 6 N hydrochloric acid before combustion at 1050°C in a HERAEUS CHN-O-Rapid elemental analyser. The relative precision of the measurements is based on duplicates as well as via control analysis of a lab internal reference sediment sample.

To aliquots of 6 to 13 g of sediment samples (Table 1) known amounts of *n*-nonadecan-2-one were added as internal standards. The sediments were extracted by Dionex^{TM} accelerated solvent extraction (ASE) using dichloromethane/methanol (9:1, v/v; three times 5 min., 70 bar, 100°C). The total lipid extracts were separated by Al_2O_3 column chromatography using hexane/dichloromethane (9:1, v/v) to elute an apolar fraction (hydrocarbons) and

dichloromethane/methanol (1:1, v/v) to elute a polar fraction. The latter fraction, containing GDGTs for the TEX_{86} and BIT analyses as well as alkenones for the $U^{K'}_{37}$ analyses, was dried under a continuous nitrogen stream, ultrasonically dissolved in a hexane/isopropanol (99:1, v/v) mixture to a concentration of ca. 2 mg mL^{-1}, and filtered through a 0.4 μm pore size PTFE filter. The fractions for GDGT analyses were analysed in duplicate using an Agilent HP1200 high performance liquid chromatography system coupled to an Agilent 6120 mass spectrometer equipped with an atmospheric pressure chemical ionization ion source (HPLC/APCI-MS) according to the method described in *Hopmans et al.* [2004] and refined as reported in *Schouten et al.* [2007b]. The TEX_{86} index was calculated using the peak areas of ions for different GDGTs. The TEX_{86} index is defined as:

$$TEX_{86} = \frac{([GDGT-2]+[GDGT-3]+[Cren'])}{([GDGT-1]+[GDGT-2]+[GDGT-3]+[Cren'])}$$

where GDGT-1, GDGT-2, and GDGT-3 indicate GDGTs containing 1, 2, and 3 cyclopentane moieties, respectively, and Cren' the crenarchaeol regio-isomer [after *Kim et al.*, 2010]. Temperatures were calculated using the calibration for subtropical and tropical oceans (GDGT index-2) by *Kim et al.* [2010]:

$$Temp_{TEX} = 68.4 \times \log(TEX_{86}) + 38.6$$

The error of the calibration equation is ±2.5°C [*Kim et al.*, 2010]. The BIT index was calculated using the peak areas of ions for different GDGTs and the following formula [after *Hopmans et al.*, 2004]:

$$BIT = \frac{([I]+[II]+[III])}{([I]+[II]+[III])+(IV)}$$

where I, II, and III indicate GDGTs without cyclic components in the structure and IV crenarchaeol. Standard deviations of GDGT indices reported in tables are calculated from

results of duplicate analyses. A consistently analysed lab internal standard sediment (core-catcher sediment from the continental slope off Namibia: GeoB 1712-4, 23.26°S 12.81°E, 998 m water depth, 1029 cm core length; recovered during R.V. Meteor cruise M20/2 [*Schulz and Participants*, 1992]) revealed a standard deviation for analyses of $Temp_{TEX}$ of 3.54% or ± 0.51°C using the calibration of *Kim et al.* [2008]. Reported standard deviation errors of some data exhibit large deviations (up to 2.9°C; Table 1) due to low content of organics, especially of GDGTs in individual sediment samples. However, $Temp_{TEX}$ data with large analytical errors generally fit into the trend depicted by adjacent more reliable $Temp_{TEX}$ data (cf. Table 1 and Figure 2). We interpret all data only outside their analytical errors.

The remaining polar fraction was reduced to dryness and saponified using 0.5 M KOH in methanol (1 mL, 85°C, 2 h). The products were extracted with *n*-hexane after addition of distilled water. After this clean-up step the polar compounds were converted to their trimethylsilyl ether derivatives before analysis in duplicates by gas chromatography with flame ionisation detection (GC-FID) for $U^{K'}_{37}$ calculation. The $U^{K'}_{37}$ is defined as

$$U_{37}^{K'} = \frac{[C_{37:2}]}{([C_{37:2}]+[C_{37:3}])},$$

where as $C_{37:2}$ and $C_{37:3}$ refers to the di- and tri-unsaturated alkenones, respectively [*Prahl and Wakeham*, 1987]. The SSTs were calculated using the equation from *Müller et al.* [1998]:

$$SST_{UK} = \frac{\left(U_{37}^{K'} - 0.044\right)}{0.033}$$

The error of the calibration equation is ±1°C [*Müller et al.*, 1998]. A consistently analysed lab internal standard sediment (GeoB 1712-4) revealed a standard deviation for analyses of SST_{UK} of 2.21% or ± 0.38°C by using the calibration of *Müller et al.* [1998].

A complete set of analytical data of this study is available through the PANGAEA database (http//www.pangaea.de/).

4. Results

TOC, SST_{UK}, and $Temp_{TEX}$ of this study are displayed in Figure 2, whereas numerical data are given in Table 1. The TOC content record ranges between 0.1 and 1.8 % and exhibits a gradual increase from 0.2 % at approximately 12 Ma to 0.7 % at 10 Ma. These relatively low values are followed by a slight overall decrease to approximately 0.4 % at 6.9 Ma and a subsequent increase to highest values of approximately 1.8 % in Pliocene sediments. TOC values of Pleistocene sediment samples (ca. 1.2 %) are slightly lower than those of the Pliocene (Figure 2).

SSTs estimated by $U^{K'}_{37}$ exhibit a monotonous decrease of about 8 degrees from maximum values of 27.5°C between 13.7 and 11.6 Ma to approximately 19°C at 2.8 Ma. $Temp_{TEX}$ values decline steeply from 30.5°C at 13.7 Ma to approximately 19°C at 9.5 Ma and then remain rather constant until 6.5 Ma. Between 6.5 and 5.0 Ma the $Temp_{TEX}$ values fluctuate between 25 and 17°C and, afterwards, the values exhibit a gradual decline from ca. 17 to 15°C at 2.8 Ma. The overall amplitude of $Temp_{TEX}$ data amounts to about 16 degrees. Pleistocene water temperature estimates of both proxies indicate temperatures of around 17.5 to 18.0°C (Figure 2, Table 1). In general, $Temp_{TEX}$ fluctuations have larger amplitudes than those of the SST_{UK} and mostly show an offset of around 4°C up to 7°C to colder temperatures. Between 6.5 and 5 Ma and during the Pleistocene SST_{UK} and $Temp_{TEX}$ are more similar (Figure 2).

5. Discussion

5.1. Significance of proxies

An organic deep-sea sediment proxy record of a time-span of over millions of years may have been affected by evolutionary changes in source organisms and/or microbial, chemical or oceanic processes like degradation, resuspension, transport, or dissolution. Therefore, we first discuss the reliability and limits of our data.

During the middle to late Miocene an effect of low TOC preservation is evident for ODP Site 1085 possibly due to oxic bottom water conditions [*Diester-Haass et al.*, 2004; *Dupont et al.*, 2011]. Although TOC is a first-order proxy for primary productivity being low during times of low productivity, preservation effects may also be reflected in TOC values, especially during the middle Miocene period (Figure 2). Organic preservation is better after 11 Ma and probably excellent between 9 and 8 Ma as well as between 6 and 5 Ma indicated by the high abundances of palynomorphs that are sensitive to oxygenic degradation [*Dupont et al.*, 2011]. Hence, middle Miocene temperature data might be biased by low preservation. Although surface productivity (upper continental slope off high upwelling areas) might be less the preservation of organic matter is enhanced in slope depocenters due to the deposition of resuspended material [*Inthorn et al.*, 2006; *Mollenhauer et al.*, 2002]. Sediments of the shelf eroded by rapid sea level changes and by dissipation of wave and tidal energy, are transported laterally in southward flowing nepheloid layers, aligned by bottom ocean currents, and deposited at the upper continental slope [*Compton and Wiltshire*, 2009; *Compton et al.*, 2009; *Mollenhauer et al.*, 2002; *Mollenhauer et al.*, 2007]. On the margin, deposition was continuous since the Middle Miocene [*Weigelt and Uenzelmann-Neben*, 2004]. On the shelf, major composite erosional unconformities occurred in the middle Miocene to Plio-/Pleistocene [*Compton et al.*, 2004]. Lateral transport of organic material may have biased our water temperature estimations, but, age-estimations resulting in offsets between organic

temperature proxies are effective only on short time scales [*Mollenhauer et al.*, 2007]. Hence, lateral transport is present, but, is negligible for our trend-observations over million of years.

5.1.1. SST_{UK}

The calibration of *Müller et al.* [1998] for the $U^{K'}_{37}$ index used in this study is based on recent sediments containing alkenones mainly produced by the haptophyte *Emiliania huxleyi*. This coccolithophorid species became the dominant alkenone-producing organism during the last 70-80 kyr and first appeared 268 kyr ago [*Thierstein et al.*, 1977]. Alkenones in sediments dating back to the Eocene (55.8 to 33.9 Ma) are attributed to extinct genera of the family *Gephyrocapsaceae*, possible ancestors of *Emiliania* [*Marlowe et al.*, 1990]. Several studies confirmed that these species produce alkenones without significant difference in SST dependence to *Emiliania* [e.g. *Conte et al.*, 1995; *McClymont et al.*, 2005; *Müller et al.*, 1997; *Villanueva et al.*, 2002]. We therefore assume that the $U^{K'}_{37}$ calibration by *Müller et al.* [1998] is applicable to Miocene samples.

The $U^{K'}_{37}$ calibration was shown to be linear over a temperature range between 0 and 27°C [*Müller et al.*, 1998]. Above this temperature as found in tropical or subtropical oceans alkenone-producing haptophytes only synthesize trace amounts of tri-unsaturated alkenones and the $U^{K'}_{37}$ becomes insensitive to temperature. Obviously the sensitivity limit is reached in our data during most of the middle Miocene, in which the SST_{UK} curve flattens and reaches its maximum value of 27.5°C (Table 1, Figure 2).

Regardless of the calibration accuracy, oxic bottom water conditions affect the di- and tri-unsaturated species to different extents, where the tri-unsaturated alkenone may be degraded faster resulting in a relative increase of $U^{K'}_{37}$ that would translate into a shift of SST_{UK} to higher values [*Gong and Hollander*, 1999; *Hoefs et al.*, 1998; *Huguet et al.*, 2009; *Kim et al.*, 2009; *Rontani et al.*, 2005; *Rontani et al.*, 2008; *Teece et al.*, 1998]. Other studies, however,

showed that the $U^{K'}_{37}$ index seems to be unaffected or that differential degradation has only a minor effect on the estimated temperature (up to 1.2 °C), despite a strong decrease in amount of alkenones [*Huguet et al.*, 2009; *Kim et al.*, 2009; *Prahl et al.*, 1989]. Oxic degradation is obvious in ODP Site 1085 sediments of the middle Miocene, where the $U^{K'}_{37}$ reached its calibration limit (Figure 2). The SST_{UK} data prior to 11 Ma are, therefore, not usable to estimate temperatures. The preservation of organic matter increased after 11 Ma when we presume the effects of post-depositional oxidation to be minor.

5.1.2. $Temp_{TEX}$

The TEX_{86} is defined as the abundance ratio of GDGTs with different numbers of cyclopentane rings, synthesized by picoplankton of the phyllum Thaumarchaeota, which was previously thought to be related to the lineage Crenarchaeota [*Schleper and Nicol*, 2010; *Schouten et al.*, 2002; *Wuchter et al.*, 2004]. Some species of the Thaumarchaeota are extremophiles (e.g., hyperthermophilic organisms) and can grow at temperatures higher than 60°C [*Blöchl et al.*, 1998; *Karner et al.*, 2001]. Marine (pelagic) species are thought to have adjusted their membrane lipids to colder environments by introducing crenarchaeol, a cyclohexane containing GDGT [*Sinninghe Damsté et al.*, 2002]. Hence, TEX_{86} is not limited by maximum surface temperatures as $U^{K'}_{37}$. Instead, it exhibits a non-linear behaviour for water temperatures below 5°C [*Kim et al.*, 2008; *Kim et al.*, 2010], which are not relevant in our study (Table 1). The TEX_{86} calibration of recent core-top sediments has been applied for water temperature reconstructions of the past 120 Myr [e.g. *Dumitrescu et al.*, 2006; *Pearson et al.*, 2007; *Schouten et al.*, 2007a; *Sluijs et al.*, 2006] and no deviations are known resulting from evolutionary effects of the source organisms. Studies on the effect of differential degradation of GDGTs deposited under oxic or anoxic sedimentary conditions are inconclusive, suggesting either a temperature bias of up to 6°C or no significant change [*Huguet et al.*, 2009; *Huguet et al.*, 2008; *Kim et al.*, 2009; *Schouten et al.*, 2004]. On the

other hand, a radiocarbon study by *Mollenhauer et al.* [2008] reveal large differences between radiocarbon contents of alkenones and crenarchaeol suggesting selective preservation of alkenones, while crenarchaeol might be degraded more rapidly in oxygenated water masses. However, since 11 Ma oxic degradation should have had relatively small effects on organic molecules used to estimate water temperatures.

A bias affecting TEX_{86}-based water temperature estimates has been observed in sediments rich in terrestrial organic matter. The ratio of soil derived GDGTs *versus* marine crenarchaeol, the BIT index, is used as a proxy of riverine transported terrestrial organic matter. In theory BIT = 0 is expected for open ocean conditions and BIT = 1 for pure terrestrial soils [*Hopmans et al.*, 2004]. *Weijers et al* [2006; 2007] reported that river run-off of terrestrial soils may contain GDGTs used for the TEX_{86} parameter and that large amounts of terrestrial organic matter associated with high BIT values may shift the TEX_{86} values towards warmer temperatures. Sediment samples of this study are potentially influenced by river run-off from the adjacent Orange River. High BIT values of around 0.88 were found for the middle Miocene (Figure 2b and Table 1) and relatively low values of around 0.13 afterwards (Table 1). A $Temp_{TEX}$ deviation of +1°C may be reached at a BIT index of 0.2–0.3 [*Weijers et al.*, 2006]. The degree of biasing depends on the GDGT composition in river discharged soil material [*Weijers et al.*, 2006]. The latter, however, is unknown. As the bias is higher for relatively low water temperatures and less so for warm waters [*Weijers et al.*, 2006] but $Temp_{TEX}$ estimates with low BIT values at that time indicate values >25°C and $U^{K'}_{37}$ values reach their calibration limit close to 28°C, we infer that the overestimation of $Temp_{TEX}$ is likely minor. This is supported by the general resemblance of the $Temp_{TEX}$ record with deep water cooling (Figure 2a). As BIT values are low during the later periods, the rest of the $Temp_{TEX}$ record is not affected by Orange River discharge. In Figure 2 we marked $Temp_{TEX}$ values (pale grey) that are associated with BIT values exceeding 0.3. Excluding these

potentially biased data points does, however, not change the general trend of steep $Temp_{TEX}$ decline during the middle to late Miocene.

5.1.3. Differences between SST_{UK} and $Temp_{TEX}$

We observe an offset between both water temperature proxies between 11 and 7 Ma as well as during the Pliocene (Figure 2), which for the above mentioned reasons we consider not to be related to differential preservation and systematic degradation of individual lipids. It is commonly assumed that alkenone- and GDGT-based temperature estimates represent water temperatures of the upper parts of the water column, because both indices correlate well with mean annual surface temperatures [e.g. *Herbert*, 2001; *Kim et al.*, 2008; *Prahl and Wakeham*, 1987; *Prahl et al.*, 2000; *Schouten et al.*, 2002]. Several studies, however, found offsets between SST_{UK} and $Temp_{TEX}$ estimates [e.g., *Huguet et al.*, 2006; *Lee et al.*, 2008; *Leider et al.*, 2010; *Lopes dos Santos et al.*, 2010]. These studies attributed the findings to different seasonal production and/or depth habitats. Alkenones are produced in the euphotic zone by haptophyte phytoplankton species, which require sunlight for photosynthesis. They may be outcompeted, e.g., by diatoms during strong upwelling of silicate-rich deep waters [*Mitchell-Innes and Winter*, 1987]. Over Site 1085, however, elevated surface productivity is supported only by filaments laterally derived from coastal perennial upwelling [*Lutjeharms and Stockton*, 1987]. The global core-top calibration of $U^{K'}_{37}$ [*Müller et al.*, 1998] contains samples from the BUS area showing no deviation from the mean annual SSTs.

High fluxes of GDGTs associated with high abundances of Thaumarchaeota have been observed to be seasonal [*Herfort et al.*, 2006; *Huguet et al.*, 2007; *Wuchter et al.*, 2005; *Wuchter et al.*, 2006]. Their blooms potentially occur as a consequence of changes in the nutrient composition triggered by rising ammonium levels related to surface productivity [*Wuchter et al.*, 2006]. Some Thaumarchaeota are autotrophic nitrifiers which oxidize

ammonium to nitrite [*Ingalls et al.*, 2006; *Könneke et al.*, 2005; *Martens-Habbena et al.*, 2009; *Wuchter et al.*, 2006]. Many studies reported that Thaumarchaeota mainly thrive in sub-surface water layers below the highly productive euphotic zone, where, potentially, the ammonium content rises to a maximum level [*Huguet et al.*, 2007; *Karner et al.*, 2001; *Murray et al.*, 1999; *Pearson et al.*, 2007; *Shah et al.*, 2008; *Wuchter et al.*, 2005].

SST_{UK} data from surface sediments of the Cape Basin as well as SSTs derived from satellite data ($SST_{satellite}$) [*Lee et al.*, 2008] agree well, whereas $Temp_{TEX}$ are biased to colder temperatures (Figure 3a). The offset between SST_{UK} and $Temp_{TEX}$ is smaller at greater water depth or at greater distance from the upwelling near the coast. Sites within strong upwelling exhibit the largest offset between both temperature proxies. TOC data of the same core-top sediments [*Inthorn et al.*, 2006] correlate to the temperature offset (ΔTemp, Figure 3b). This suggests that ΔTemp depends on the degree of marine primary productivity in the surface waters. We calculated a ΔTemp of our data based on reliable temperature estimates without SST_{UK} close to the calibration limit and $Temp_{TEX}$ accompanied by BIT > 0.3 (Figure 2c) to avoid any potentially biased temperature estimates. Comparing the Miocene to Pliocene records of ΔTemp and TOC (Figure 2d), however, no correlation is observed despite good preservation of organic matter since 11 Ma. The highest ΔTemp is indeed observed during the first increase of TOC at around 11 Ma, but the high TOC values around 6 Ma are not associated to a high ΔTemp and, instead, correlate to similar SST_{UK} and $Temp_{TEX}$ values. Elevated primary productivity alone can thus not explain the temperature offset. Apparently, elevated surface water primary productivity only causes displacement of Thaumarchaeota to sub-surface water layers but temperature variations recorded in the sub-surface layers are primarily driven by other processes. Interestingly, $Temp_{TEX}$ values in our study never decrease below 15°C, which is the present temperature at the base of the surface water layer extending to around 400 meters water depth [*Schneider et al.*, 2003]. We thus infer, that

$Temp_{TEX}$ in the Cape Basin records sub-surface water temperatures below the surface mixed layer but above the permanent thermocline. In a recent study by *Lopes dos Santos et al.* [2010] in the eastern tropical Atlantic a similar conclusion was drawn that $Temp_{TEX}$ records thermocline temperatures and connections were made between thermocline adjustments and the strength of the meridional overturning circulation.

5.2. Development of the Benguela upwelling system (BUS)

5.2.1. Onset and intensification of upwelling

The high-resolution stable oxygen isotope record ($\delta^{18}O$) of benthic foraminifera from ODP Site 1085 (Figure 2a) indicates Antarctic ice growth and global cooling until 10 Ma associated with cooling of bottom waters at ODP Site 1085 [*Westerhold et al.*, 2005]. Both late Miocene to Pliocene temperature data sets of this study show a trend to cooler temperatures over 11 Myr (Figure 2b). In conjunction with the benthic $\delta^{18}O$ data, the temperature signals represent a record of increasing impact of cold waters of Antarctic origin on surface and sub-surface waters of the Southeast Atlantic Ocean. $Temp_{TEX}$ values agree better with benthic oxygen isotopic values compared to SST_{UK} values. It seems that the $Temp_{TEX}$ record is more strongly affected by changes in temperatures of southern sourced cold water. The SST_{UK} development, on the other hand, indicates a more gradual cooling in the upper water layers at ODP Site 1085 consisting of ocean surface waters mixed with waters of filaments derived from coastal upwelling areas.

Large temperature shifts between 3°C and 10°C since the middle Miocene climatic optimum (16 Ma) were found by several studies outside of the BUS [*Billups and Schrag*, 2002; *Browning et al.*, 2006; *Flower and Kennett*, 1994; *Miller et al.*, 1991; *Shevenell et al.*, 2004; *Williams et al.*, 2005], while largest differences between late Miocene and modern water temperatures occurred at low latitudes of the Southern Hemisphere [*Williams et al.*,

2005]. In the Eastern Pacific, nearly 50% of the diatom assemblages were replaced by cold-water species during a major middle Miocene cooling from 14.9 to 12.4 Ma, reflecting increased upwelling and cooling of surface waters [*Barron and Baldauf*, 1990]. Increased Antarctic glaciations promoting intermediate and bottom water formation [*Diekmann et al.*, 2003] and intensification of the Hadley circulation [*Flohn*, 1978], combined with an intensified Southern Hemisphere southeast wind system, [*Roters and Henrich*, 2010] are inferred causes. Both mechanisms intensified upwelling at the west coasts of the Southern Hemisphere continents. Unfortunately, the lack of reliable temperature estimations for the middle Miocene does not allow dating the start of the cooling trend in the Benguela system, which might have started in the Cape Basin during the early to middle Miocene [cf. *Compton et al.*, 2004].

Between 11 and 9 Ma the offset between SST_{UK} and $Temp_{TEX}$ increased steeply to a maximum of 7°C at 9.5 Ma and declined and levelled off to 4°C on average afterwards (Figure 2c). We interpret this as increased inflow of cold and nutrient-rich intermediate Antarctic waters to the Cape Basin. Between 11 and 10 Ma, the increase of TOC values indicate the start of enhanced marine primary productivity (Figure 2d) which is substantiated by TOC data and foraminifera counts by *Diester-Haass et al.* [2004]. During the TOC maximum between 9.5 and 9 Ma the largest difference between both temperature proxies of up to 7°C is found. We interpret this as the result of cold Antarctic intermediate water advection being overlain by cool surface water filaments originating at the upwelling centers along the coast of the southern BUS. At ODP Site 1085 water of upwelling filaments would have caused changes in surface productivity and the TEX source organisms would have been displaced to sub-surface water layers by a gradual increase of the primary productivity in the surface waters. A downward shift of the GDGT source-organisms would have resulted in an increasing offset between the two temperature estimates from 11 to 9 Ma (Figure 2b and c).

By 9 Ma, the upwelling system seems to have been established resulting in an average temperature difference of approximately 4°C between surface and sub-surface waters over Site 1085.

5.2.2. Changes in Atlantic Ocean circulation

Progressive intensification of upwelling of cold and nutrient rich Antarctic waters from late Miocene to Pliocene times is reflected by an overall increase in TOC as well as a parallel cooling in SST_{UK} and $Temp_{TEX}$ since 10 Ma, except during the period between 6.5 and 5.0 Ma (Figure 2). At 7 Ma $Temp_{TEX}$ converge with SST_{UK} and records similar or even higher water temperatures until 5 Ma indicating warming of sub-surface waters (Figure 2b). Based on the hitherto interpretation, similar surface and sub-surface temperatures could indicate a strong decline in upwelling, which is, however, inconsistent with the relatively high and rising TOC values in combination with high accumulation rates of benthic foraminifera suggesting high marine primary productivity at ODP Site 1085 during this period [*Diester-Haass et al.*, 2002; *Diester-Haass et al.*, 2004] (Figure 2). The high marine productivity at ODP Site 1085 is not a local, but part of global phenomenon [*Diekmann et al.*, 2003; *Diester-Haass et al.*, 2002], which is called the "biogenic bloom" event [e.g., *Dickens and Owen*, 1999; *Farrell et al.*, 1995]. It has been suggested that changes in intermediate waters caused fundamental changes in the nutrient cycling during this event.

An explanation for the detected sub-surface warming between 6.5 and 5.0 Ma may be related to variability in the strength of North Atlantic deep-water formation on the temperatures of the intermediate waters of the South Atlantic. The existence of Northern Component Deep Water since the late Miocene is assumed by many authors [*Berger and Wefer*, 1996a; *Diester-Haass et al.*, 2004; *Frank et al.*, 2002; *Robert et al.*, 2005; *Woodruff and Savin*, 1989]. Deep water exchange between the Pacific and Atlantic Ocean was restricted

long before the final closure of the Central American Seaway in the Pliocene and might have stimulated North Atlantic deep-water production since the late Miocene [*Molnar*, 2008; *Schneider and Schmittner*, 2006]. *Lee et al.* [2008] document that at present, when the North Atlantic deep-water formation is strong, SST_{UK} and $Temp_{TEX}$ show an offset in the Cape Basin. Conversely, the reduction of sub-surface heat export from the South Atlantic and deepening of the thermocline due to a reduction in the rate of North Atlantic deep-water formation would decrease the offset between both temperature proxies. A sub-surface warming and a downward mixing of heat from the South Atlantic thermocline has been observed during times of reduced North Atlantic deep-water formation [*Huang et al.*, 2000; *Rühlemann et al.*, 2004]. Models indicate that the warming of the South Atlantic resulting from reduced deepwater formation is most pronounced in the sub-surface waters extending to 30°S [e.g. *Dahl et al.*, 2005; *Haarsma et al.*, 2008; *Huang et al.*, 2000; *Rühlemann et al.*, 2004; *Vellinga and Wood*, 2002]. While the continuous cooling of surface waters in combination with high surface productivity suggests enhanced upwelling, sub-surface water temperatures might have increased as a consequence of reduced North Atlantic deep-water formation. Hence, the convergence of both temperature proxies between 6.5 and 5 Ma would be the result of cooler surface temperatures and warmer sub-surface ones. Similarly, *Lopes dos Santos et al.* [2010] attributed changes in the offset between SST_{UK} and $Temp_{TEX}$ in the eastern equatorial Atlantic to variations in the strength of the Atlantic overturning circulation.

The dating of events related to the Messinian Salinity Crisis corresponds to the period for which we observe convergence of surface and sub-surface water temperature estimates (6.5 to 5.0 Ma; Figure 2b). The isolation of the Mediterranean Sea and the cessation of the inflow of salty Mediterranean water into the Atlantic Ocean was originally dated between 5.96 and 5.33 Ma [e.g. *Hilgen et al.*, 2007; *Krijgsman et al.*, 1999; *Roveri et al.*, 2008]. However, *Van Assen et al.* [2006] found evidence that the input of Atlantic waters into the Mediterranean Sea

became restricted much earlier, already by 6.84 Ma. Decrease of the salt water input into the Atlantic would have decreased deepwater formation and thus weakened Atlantic overturning circulation [e.g. *Barreiro et al.*, 2008]. We, therefore, interpret the strong sub-surface warming observed in $Temp_{TEX}$ between 6.5 and 5 Ma indicating a downward mixing of heat from the thermocline as an effect of reduced North Atlantic deep-water formation in association with the reduced salt import into the Atlantic Ocean during the Messinian Salinity Crisis.

Also for the Pleistocene samples, no offset between both temperature proxies (SST_{UK} and $Temp_{TEX}$) exists, while TOC is at the same relatively high level as during the late Pliocene (Figure 2b,c,d). All three Pleistocene samples used for comparison are from the last Glacial when North Atlantic deep-water formation was weak, South Atlantic subsurface waters were relatively warm and the thermocline shifted downward [cf. *Lopes dos Santos et al.*, 2010; *Rühlemann et al.*, 2004]. This observation is consistent with our proposed scenario that differences between in the Benguela current system reflect the strength of North Atlantic deep-water formation.

5.2.3. Intensification of Northern Hemisphere glaciation

Since 5 Ma the Northern Hemisphere converted into permanently glaciated conditions with fluctuating ice sheets, which is linked to further uplift of the Isthmus of Panama and, finally, to the closure of the Central American Seaway at around 2.7 to 2.6 Ma [*Haug and Tiedemann*, 1998; *Larsen et al.*, 1994; *Molnar*, 2008; *Zachos et al.*, 2001]. The closure of the Seaway caused intensification of the North Atlantic deep-water formation which resulted in enhanced heat export from the South Atlantic [*Haug and Tiedemann*, 1998; *Klocker et al.*, 2005] as well as amplification of Milankovitch cycles starting around 3 Ma [*Fedorov et al.*, 2006]. Additionally, strengthening of global major currents led to a northward shift of the

Antarctic polar front and the Subtropical Convergence Zone in the South Atlantic, which might have resulted in an increase in velocity of the BUS [*Diester-Haass*, 1988; *Diester-Haass and Rothe*, 1987], changes in zonal temperature gradients, and major changes in mid-latitudinal SST [*Brierley and Fedorov*, 2010]. The ocean heat fluxes probably responded to changes in atmospheric winds [*Barreiro et al.*, 2008; *Boccaletti et al.*, 2005]. Intensification of trade winds are, therefore, expected to initiate a positive feedback and to enhance coastal upwelling intensity [*Marlow et al.*, 2000]. In the Southeast Atlantic, evidence for trade wind intensification is provided by the parallel decrease of both, SST_{UK} and $Temp_{TEX}$ values from approximately 5 to 2.8 Ma (Figure 2b), as well as by increasing TOC values, which point to further enhancement of marine productivity (Figure 2d) [*Diester-Haass et al.*, 2004].

At ODP Site 1084 offshore Lüderitz, which today is situated under the highest productive cell of the BUS around 5° of latitude north of ODP Site 1085 (Figure 1), *Marlow et al.* [2000] found SST_{UK} values of approximately 26°C to 27°C from 4.6 to 3.2 Ma decreasing to fluctuating values between 12 and 18°C for the late Pleistocene (Figure 2b). In contrast, our results imply cooler SST_{UK} of around 21°C until about 3.9 Ma followed by a gradual decrease to 19°C until 2.8 Ma and by a shift to about 16 and 19°C in the Pleistocene (Figure 2b), similar to values found by *Lee et al.* [2008]. We interpret this as a northward shift of the area of strongest upwelling to a position offshore Lüderitz during the Pliocene, which is suggested by the further cooling of SST_{UK} after 3 Ma. This implies that strengthening of upwelling intensity started in the southern BUS and progressed northward later on. Possibly, a northward shift of strong upwelling areas occurred due to further expansion of polar ice sheets and corresponding frontal systems.

6. Summary and conclusions

Two organic molecular proxies for ocean temperatures were used in conjunction with TOC content and published data from ODP Site 1085 to identify the history of the BUS in the Southeast Atlantic Ocean from Miocene to Pliocene times. In concordance with global cooling from the Miocene climatic optimum to the Pliocene, both, SST_{UK} and $Temp_{TEX}$ temperature proxies exhibit a cooling trend between 13.7 and 2.8 Ma with a significant overall shift of 8°C and 16°C, respectively. Temperature trends depicted by both proxies differ in rate and timing, which may be related to different habitats of their source organisms. The SST_{UK} data reflect the warmer surface water temperatures of the euphotic zone, while $Temp_{TEX}$ data likely reflect colder sub-surface waters. Increased primary productivity presumably leads to migration of the GDGTs source-organisms ($Temp_{TEX}$) to sub-surface waters below the surface mixed layer.

$Temp_{TEX}$ exhibit a similar temporal trend as $\delta^{18}O$ of benthic foraminifera likely indicating advection of cold Antarctic intermediate waters, the latter influencing sub-surface water temperatures. SST_{UK} data record a more gradual decrease in surface temperatures. We suggest that intensified Benguela upwelling during the Miocene led to a gradual decrease in sea surface temperatures over ODP Site 1085 by mixing with cold waters from filaments originating from coastal upwelling. Rapid cooling of sub-surface waters and an increase in marine productivity after 11 Ma points to intensified upwelling in the southern Benguela system, while a significant offset between both temperature proxies developed at 10 Ma.

During the period of the Mediterranean Salinity Crisis (6.8 to 5.3 Ma) a rapid warming of sub-surface waters to temperatures similar to or exceeding those of the surface waters suggests deepening of the thermocline as the result of decreased Atlantic overturning circulation due to decrease or cessation of salt input from the Mediterranean Sea into the Atlantic Ocean.

Parallel cooling of surface and sub-surface waters resumed in the Pliocene, when the Northern Hemisphere glaciations intensified.

7. Acknowledgements

We thank Dr. Martin Butzin (University of Bremen, Germany), Dr. Torsten Bickert (University of Bremen, MARUM, Germany), Dr. Gregor Knorr (Alfred-Wegener-Institute, Bremerhaven, Germany), Dr. Stephan Mulitza (University of Bremen, MARUM, Germany) and Prof. Dr. Gerrit Lohmann (Alfred-Wegener-Institute, Bremerhaven, Germany) for helpful advice and constructive discussion as well as Ralph Kreutz and Hella Buschhoff (both from University of Bremen, Germany), Elke Joost, Katharina Siedenberg and Abhinav Gogoi (all MARUM, University of Bremen, Germany) for analytical support. Prof. Dr. John Compton (University of Cape Town, Republic of South Africa), Prof. Dr. Jaap S. Sinninghe Damsté (Royal Netherlands Institute for Sea Research, Netherlands) and an anonymous referee are gratefully acknowledged for constructive reviews. Samples were taken at the ODP repository in Bremen. Data are archived in PANGAEA <www.pangaea.de>. This study was financially supported by the Deutsche Forschungsgemeinschaft (DFG, Bonn, Germany) within the research unit "Understanding Cenozoic Climate Cooling: The Role of the Hydrology Cycle, the Carbon Cycle, and Vegetation Changes" (FOR 1070), Grant no. SCHE 903/6.

8. References

Andrews, W. R. H., and L. Hutchings (1980), Upwelling in the Southern Benguela Current, *Prog. Oceanogr.*, *9*, 1-81.

Barreiro, M., A. Fedorov, R. Pacanowski, and S. G. Philander (2008), Abrupt climate changes: How freshening of the northern Atlantic affects the thermohaline and wind-driven oceanic circulations, *Annu. Rev. Earth Pl. Sc.*, *36*, 33-58.

Barron, J. A., and J. G. Baldauf (1990), Development of biosiliceous sedimentation in the North Pacific during the Miocene and early Pliocene, in *Neogene Events: Their Timing,*

Nature and Interrelationship, edited by R. Tsuchi, pp. 43-63, University of Tokyo Press, Tokyo.

Berger, W. H. (1989), Global maps of ocean productivity, in *Productivity in the Ocean: Present and Past*, edited by W. H. Berger, V. S. Smetacek and G. Wefer, pp. 429-455, Dahlem Conf. John Wiley, Chichester.

Berger, W. H., and G. Wefer (1996a), Expeditions into the past: Paleoceanographic studies in the South Atlantic, in *The South Atlantic: Present and Past Circulation*, edited by G. Wefer, W. H. Berger and G. Siedler, pp. 363-410, Springer-Verlag, Berlin.

Berger, W. H., and G. Wefer (1996b), Central themes of South Atlantic circulation, in *The South Atlantic: Present and Past Circulation*, edited by G. Wefer, W. H. Berger, G. Siedler and D. J. Webb, pp. 1-11, Springer-Verlag, Berlin.

Berger, W. H., C. B. Lange, and G. Wefer (2002), Upwelling history of the Benguela-Namibia system: a synthesis of Leg 175 results, in *Proceedings of the Ocean Drilling Program, Scientific Results*, edited by G. Wefer, W. H. Berger and C. Richter, College Station, Texas.

Billups, K., and D. P. Schrag (2002), Paleotemperatures and ice volume of the past 27 Myr revisited with paired Mg/Ca and O-18/O-16 measurements on benthic foraminifera, *Paleoceanography, 17*(1).

Blöchl, E., R. Rachel, S. Burggraf, D. Hafenbrandl, H. W. Jannasch, and K. O. Stetter (1998), *Pyrolobus fumarii*, gen. and sp. nov., represents a novel group of archaea, extending the upper temperature limit for life to 113°C, *Extremophiles*, *1*(14-21).

Boccaletti, G., R. Ferrari, A. Adcroft, D. Ferreira, and J. Marshall (2005), The vertical structure of ocean heat transport, *Geophys. Res. Lett.*, *32*(10), -.

Brassell, S. C., G. Eglinton, I. T. Marlowe, U. Pflaumann, and M. Sarnthein (1986), Molecular stratigraphy: a new tool for climatic assessment, *Nature, 320*, 129-133.

Bremner, J. M., J. Rogers, and J. P. Willis (1990), Sedimentological Aspects of the 1988 Orange River Floods, *Trans. R. Soc. S. Afr., 47*, 247-294.

Brierley, C. M., and A. V. Fedorov (2010), Relative importance of meridional and zonal sea surface temperature gradients for the onset of the ice ages and Pliocene-Pleistocene climate evolution, *Paleoceanography, 25*, -.

Broecker, W. S., D. M. Peteet, and D. Rind (1985), Does the Ocean-Atmosphere System Have More Than One Stable Mode of Operation, *Nature, 315*(6014), 21-26.

Browning, J. V., K. G. Miller, P. P. McLaughlin, M. A. Kominz, P. J. Sugarman, D. Monteverde, M. D. Feigenson, and J. C. Hernandez (2006), Quantification of the effects of eustasy, subsidence, and sediment supply on Miocene sequences, mid-Atlantic margin of the United States, *Geol. Soc. Am. Bull.*, *118*(5-6), 567-588.

Compton, J. S., and J. G. Wiltshire (2009), Terrigenous sediment export from the western margin of South Africa on glacial to interglacial cycles, *Mar. Geol.*, *266*(1-4), 212-222.

Compton, J. S., R. Wigley, and I. K. McMillan (2004), Late Cenozoic phosphogenesis on the western shelf of South Africa in the vicinity of the Cape Canyon, *Mar. Geol.*, *206*(1-4), 19-40.

Compton, J. S., C. T. Herbert, and R. Schneider (2009), Organic-rich mud on the western margin od southern Africa: Nutrient source to the Southern Ocean?, *Global Biogeochem. Cy.Cycles*, *23*, 12pp.

Conte, M. H., A. Thompson, G. Eglinton, and J. C. Green (1995), Lipid Biomarker Diversity in the Coccolithophorid Emiliania-Huxleyi (Prymnesiophyceae) and the Related Species Gephyrocapsa-Oceanica, *J. Phycol.*, *31*(2), 272-282.

Dahl, K., A. Broccoli, and R. Stouffer (2005), Assessing the role of North Atlantic freshwater forcing in millennial scale climate variability: a tropical Atlantic perspective, *Clim. Dynam.*, *24*(4), 325-346.

Dickens, G. R., and R. M. Owen (1999), The Latest Miocene-Early Pliocene biogenic bloom: a revised Indian Ocean perspective, *Mar. Geol.*, *161*(1), 75-91.

Diekmann, B., M. Falker, and G. Kuhn (2003), Environmental history of the south-eastern South Atlantic since the Middle Miocene: evidence from the sedimentological records of ODP Sites 1088 and 1092, *Sedimentology*, *50*(3), 511-529.

Diester-Haass, L. (1988), Sea-Level Changes, Carbonate Dissolution and History of the Benguela Current in the Oligocene Miocene Off Southwest Africa (Dsdp Site-362, Leg-40), *Mar. Geol.*, *79*(3-4), 213-242.

Diester-Haass, L., and P. Rothe (1987), Plio-Pleistocene Sedimentation on the Walvis Ridge, Southeast Atlantic (Dsdp Leg-75, Site-532) - Influence of Surface Currents, Carbonate Dissolution and Climate, *Mar. Geol.*, *77*(1-2), 53-&.

Diester-Haass, L., P. A. Meyers, and P. Rothe (1990), Miocene history of the Benguela current and Antarctic ice volumes: evidence from rhythmic sedimentation and current growth across the Walvis Ridge (Deep Sea Drilling Project sites 362 and 532, *Paleoceanography*, *5*, 685-707.

Diester-Haass, L., P. A. Meyers, and L. Vidal (2002), The late Miocene onset of high productivity in the Benguela Current upwelling system as part of a global pattern, *Mar. Geol.*, *180*(1-4), 87-103.

Diester-Haass, L., P. A. Meyers, and T. Bickert (2004), Carbonate crash and biogenic bloom in the late Miocene: Evidence from ODP Sites 1085, 1086, and 1087 in the Cape Basin, southeast Atlantic Ocean, *Paleoceanography*, *19*(1), -.

Dumitrescu, M., S. C. Brassell, S. Schouten, E. C. Hopmans, and J. S. S. Damste (2006), Instability in tropical Pacific sea-surface temperatures during the early Aptian, *Geology*, *34*(10), 833-836.

Dupont, L., P. Linder, F. Rommerskirchen, and E. Schefuss (2011), Climate-driven rampant speciation of the Cape flora, *Journal of Biogeography* 10 pp.

Farrell, J. W., I. Raffi, T. R. Janecek, D. W. Murray, M. Levitan, K. A. Dadey, K.-C. Emeis, M. Lyle, J.-A. Flores, and S. Hovan (1995), Late Neogene sedimentation patterns in the eastern equatorial Pacific Ocean, *Proceedings in the Ocean Drilling Program, Scientific Results*, *138*(717–756).

Fedorov, A. V., P. S. Dekens, M. McCarthy, A. C. Ravelo, P. B. deMenocal, M. Barreiro, R. C. Pacanowski, and S. G. Philander (2006), The Pliocene paradox (mechanisms for a permanent El Nino), *Science*, *312*(5779), 1485-1489.

Flohn, H. (1978), Comparision of Antarctic and Arctic climate and its relevance to climatic evolution, in *Antarctic Glacial History and World Paleoenvironments*, edited by E. M. van Zinderen Bakker, pp. 3-13, Balkema, Rotterdam.

Flower, B. P., and J. P. Kennett (1994), The Middle Miocene Climatic Transition - East Antarctic Ice-Sheet Development, Deep-Ocean Circulation and Global Carbon Cycling, *Palaeogeogr. Palaeoclimatol. Palaeoecol.*, *108*(3-4), 537-555.

Frank, M., N. Whiteley, S. Kasten, J. R. Hein, and K. O'Nions (2002), North Atlantic DeepWater export to the Southern Ocean over the past 14 Myr: Evidence from Nd and Pb isotopes in ferromanganese crusts, *Paleoceanography*, *17*(2), 1022.

Gersonde, R., D. A. Hodell, and P. Blum (1999), Proceedings of the ODP, Initial Reports 177, edited, http://www-odp.tamu.edu/publications/177_IR/.

Gong, C., and D. J. Hollander (1999), Evidence for differential degradation of alkenones under contrasting bottom water oxygen conditions: Implication for paleotemperature reconstruction, *Geochim. Cosmochim. Acta*, *63*(3-4), 405-411.

Haarsma, R. J., E. Campos, W. Hazeleger, and C. Severuns (2008), Influence of the meridional overturning circulation on tropical Atlantic climate and variability, *J. Clim.*, *21*(6), 1403-1416.

Hart, T. J., and R. T. Currie (1960), The Benguela Current, *Discovery Report, 31*, 123-298.

Haug, G. H., and R. Tiedemann (1998), Effect of the formation of the Isthmus of Panama on Atlantic Ocean thermohaline circulation, *Nature*, *393*(6686), 673-676.

Herbert, T. D. (2001), Review of alkenone calibrations (culture, water column, and sediments), *G3 (Geochem., Geophys., Geosyst.), 2*, doi: Paper number 2000GC000055.

Herbert, T. D., and J. D. Schuffert (1998), Alkenone unsaturation estimates of late Miocene through late Pliocene sea-surface temperatures at Site 958, *Proc. Ocean Drill. Program Sci. Results*, *159T*, 17-21.

Herfort, L., S. Schouten, J. P. Boon, and J. S. Sinninghe Damsté (2006), Application of the TEX_{86} temperature proxy in the southern North Sea, *Org. Geochem.*, *37*, 1715-1726.

Hilgen, F., K. Kuiper, W. Krijgsman, E. Snel, and E. van der Laan (2007), Astronomical tuning as the basis for high resolution chronostratigraphy: the intricate history of the Messinian Salinity Crisis, *Stratigraphy*, *4*(2-3), 231-238.

Hoefs, M. J. L., G. J. M. Versteegh, W. I. C. Rijpstra, J. W. de Leeuw, and J. S. S. Damste (1998), Postdepositional oxic degradation of alkenones: Implications for the measurement of palaeo sea surface temperatures, *Paleoceanography*, *13*(1), 42-49.

Hopmans, E. C., J. W. H. Weijers, E. Schefuss, L. Herfort, J. S. S. Damste, and S. Schouten (2004), A novel proxy for terrestrial organic matter in sediments based on branched and isoprenoid tetraether lipids, *Earth Planet. Sci. Lett.*, *224*(1-2), 107-116.

Huang, R. X., M. A. Cane, N. Naik, and P. Goodman (2000), Global adjustment of the thermocline in response to deepwater formation, *Geophys. Res. Lett.*, *27*(6), 759-762.

Huguet, C., J. H. Kim, J. S. S. Damste, and S. Schouten (2006), Reconstruction of sea surface temperature variations in the Arabian Sea over the last 23 kyr using organic proxies (TEX86 and U-37(K ')), *Paleoceanography*, *21*(3), -.

Huguet, C., J. H. Kim, G. J. de Lange, J. S. Sinninghe Damsté, and S. Schouten (2009), Effects of long term oxic degradation on the $U^{K'37}$, TEX_{86} and BIT organic proxies, *Org. Geochem.*, *40*, 1188-1194.

Huguet, C., A. Schimmelmann, R. Thunell, L. J. Lourens, J. S. S. Damste, and S. Schouten (2007), A study of the TEX86 paleothermometer in the water column and sediments of the Santa Barbara Basin, California, *Paleoceanography*, *22*(3), -.

Huguet, C., G. J. de Lange, O. Gustafsson, J. J. Middelburg, J. S. S. Damste, and S. Schouten (2008), Selective preservation of soil organic matter in oxidized marine sediments (Madeira Abyssal Plain), *Geochim. Cosmochim. Acta*, *72*(24), 6061-6068.

Ingalls, A. E., S. R. Shah, R. L. Hansman, L. I. Aluwihare, G. M. Santos, E. R. M. Druffel, and A. Pearson (2006), Quantifying archaeal community autotrophy in the mesopelagic ocean using natural radiocarbon, *Proc. Natl. Acad. Sci. U. S. A.*, *103*(17), 6442-6447.

Inthorn, M., T. Wagner, G. Scheeder, and M. Zabel (2006), Lateral transport controls distribution, quality, and burial of organic matter along continental slopes in high-productivity areas, *Geology*, *34*(3), 205-208.

Karner, M. B., E. F. DeLong, and D. M. Karl (2001), Archaeal dominance in the mesopelagic zone of the Pacific Ocean, *Nature*, *409*(6819), 507-510.

Kim, J. H., S. Schouten, E. C. Hopmans, B. Donner, and J. S. S. Damste (2008), Global sediment core-top calibration of the TEX86 paleothermometer in the ocean, *Geochim. Cosmochim. Acta*, *72*(4), 1154-1173.

Kim, J. H., C. Huguet, K. A. F. Zonneveld, G. J. M. Versteegh, W. Roeder, J. S. S. Damste, and S. Schouten (2009), An experimental field study to test the stability of lipids used for the TEX86 and U-37(K ') palaeothermometers, *Geochim. Cosmochim. Acta*, *73*(10), 2888-2898.

Kim, J. H., J. van der Meer, S. Schouten, P. Helmke, V. Willmott, F. Sangiorgi, N. Koc, E. C. Hopmans, and J. S. Sinninghe Damsté (2010), New indices and calibrations derived from the distribution of crenarchaeal isoprenoid tetraether lipids: Implications for past sea surface temperature reconstructions, *Geochim. Cosmochim. Acta*, *74*(16), 4639-4654.

Klocker, A., M. Prange, and M. Schulz (2005), Testing the influence of the Central American Seaway on orbitally forced northern hemisphere glaciation, *Geophys. Res. Lett.*, *32*(3), -.

Könneke, M., A. E. Bernhard, J. R. de la Torre, C. B. Walker, J. B. Waterbury, and D. A. Stahl (2005), Isolation of an autotrophic ammonia-oxidizing marine archaeon, *Nature*, *437*(7058), 543-546.

Krammer, R., K. H. Baumann, and R. Hennich (2006), Middle to late Miocene fluctuations in the incipient Benguela Upwelling System revealed by calcareous nannofossil assemblages (ODP Site 1085A), *Palaeogeogr. Palaeoclimatol. Palaeoecol.*, *230*(3-4), 319-334.

Krijgsman, W., F. J. Hilgen, I. Raffi, F. J. Sierro, and D. S. Wilson (1999), Chronology, causes and progression of the Messinian salinity crisis, *Nature*, *400*, 652-655.

Kroopnick, P. M. (1985), The Distribution of C-13 of Sigma-Co2 in the World Oceans, *Deep-Sea Research Part a-Oceanographic Research Papers*, *32*(1), 57-84.

Kuhnert, H., T. Bickert, and H. Paulsen (2009), Southern Ocean frontal system changes precede Antarctic ice sheet growth during the middle Miocene, *Earth Planet. Sci. Lett.*, *284*(3-4), 630-638.

Larsen, H. C., A. D. Saunders, P. D. Clift, J. Beget, W. Wei, S. Spezzaferi, and O. L. S. Party (1994), Seven Million Years of Glaciation in Greenland, *Science*, *264*, 952-955.

Lear, C. H., H. Elderfield, and P. A. Wilson (2000), Cenozoic deep-sea temperatures and global ice volumes from Mg/Ca in benthic foraminiferal calcite, *Science*, *287*(5451), 269-272.

Lee, K. E., J. H. Kim, I. Wilke, P. Helmke, and S. Schouten (2008), A study of the alkenone, TEX86, and planktonic foraminifera in the Benguela Upwelling System: Implications for past sea surface temperature estimates, *Geochem., Geophys., Geosyst.*, *9*, -.

Leider, A., K.-U. Hinrichs, G. Mollenhauer, and G. J. M. Versteegh (2010), Core-top calibration of the lipid-based $U^{K'37}$ and TEX_{86} temperature proxies on the southern Italian shelf (SW Adriatic Sea, Gulf of Taranto), *Earth Planet. Sci. Lett.*, *300*(1-2), 112-124.

Leroux, M. (1983), The climate of tropical Africa, edited, pp. 39-45, Champion Press, Paris.

Locarnini, R. A., A. V. Mishonov, J. I. Antonov, T. P. Boyer, H. E. Garcia, O. K. Baranova, M. M. Zweng, and D. R. Johnson (2010), *World Ocean Atlas 2009, Volume 1: Temperature*, 184 pp., U.S. Government Printing Office, Washington, D.C.

Lopes dos Santos, R., M. Prange, I. S. Castaneda, E. Schefuß, S. Mulitza, M. Schulz, E. A. Niedermeyer, J. S. Sinninghe Damsté, and S. Schouten (2010), Glacial-interglacial variability in Atlantic Meridional Overturning Circulation and thermocline adjustment in the tropical North Atlantic, *Earth Planet. Sci. Lett.*, *300*(3-4), 407-414.

Lutjeharms, J. R. E., and J. M. Meeuwis (1987), The extent and variability of South-East Atlantic upwelling, *South African Journal of Marine Science*, *5*, 51-62.

Lutjeharms, J. R. E., and P. L. Stockton (1987), Kinematics of the upwelling front off Southern Africa, in *The Benguela and Comparable Ecosystems*, edited by A. I. L. Payne, J. A. Guland and K. H. Brink, pp. 35-49, South African Journal of Marine Science.

Marlow, J. R., C. B. Lange, G. Wefer, and A. Rosell-Melé (2000), Upwelling intensification as part of the Pliocene-Pleistocene climate transition, *Science*, *290*, 2288-2291.

Marlowe, I. T., S. C. Brassell, G. Eglinton, and J. C. Green (1990), Long-Chain Alkenones and Alkyl Alkenoates and the Fossil Coccolith Record of Marine-Sediments, *Chem. Geol.*, *88*(3-4), 349-375.

Martens-Habbena, W., P. M. Berube, H. Urakawa, J. R. de la Torre, and D. A. Stahl (2009), Ammonia oxidation kinetics determine niche separation of nitrifying Archaea and Bacteria, *Nature*, *461*(7266), 976-U234.

McClymont, E. L., A. Rosell-Mele, J. Giraudeau, C. Pierre, and J. M. Lloyd (2005), Alkenone and coccolith records of the mid-Pleistocene in the south-east Atlantic: Implications for the U-37(K) index and South African climate, *Quat. Sci. Rev.*, *24*(14-15), 1559-1572.

Miller, K. G., J. D. Wright, and R. G. Fairbanks (1991), Unlocking the Ice House - Oligocene-Miocene Oxygen Isotopes, Eustasy, and Margin Erosion, *Journal of Geophysical Research-Solid Earth and Planets*, *96*(B4), 6829-6848.

Mitchell-Innes, B. A., and A. Winter (1987), Coccolithophores - a Major Phytoplankton Component in Mature Upwelled Waters Off the Cape Peninsula, South-Africa in March, 1983, *Marine Biology*, *95*(1), 25-30.

Mollenhauer, G., T. I. Eglinton, E. C. HopmanSd, and J. S. S. Damste (2008), A radiocarbon-based assessment of the preservation characteristics of crenarchaeol and alkenones from continental margin sediments, *Org. Geochem.*, *39*(8), 1039-1045.

Mollenhauer, G., R. R. Schneider, P. J. Müller, V. Spieß, and G. Wefer (2002), Glacial/interglacial variability in the Benguela upwelling system: spatial distribution and budgets of organic carbon accumulation, *Global Biogeochem. Cy. Cycles*, *16*, 81-81-81-15.

Mollenhauer, G., M. Inthorn, T. Vogt, M. Zabel, J. S. S. Damste, and T. I. Eglinton (2007), Aging of marine organic matter during cross-shelf lateral transport in the Benguela upwelling system revealed by compound-specific radiocarbon dating, *Geochem., Geophys., Geosyst., 8*, -.

Molnar, P. (2008), Closing of the Central American Seaway and the ice age: A critical review, *Paleoceanography*, *23*(1), -.

Müller, P. J., M. Cepek, G. Ruhland, and R. R. Schneider (1997), Alkenone and coccolithophorid species changes in late Quaternary sediments from the Walvis Ridge: implications for the alkenone paleotemperature method, *Palaeogeogr., Palaeoclim., Palaeoecol., 135*, 71-96.

Müller, P. J., G. Kirst, G. Ruhland, I. von Storch, and A. Rosell-Melé (1998), Calibration of the alkenone paleotemperature index $U^{k'}_{37}$ based on core-tops from the eastern South Atlantic and the global ocean (60°N-60°S), *Geochim. Cosmochim. Acta, 62*, 1757-1772.

Murray, A. E., A. Blakis, R. Massana, S. Strawzewski, U. Passow, A. Alldredge, and E. F. DeLong (1999), A time series assessment of planktonic archaeal variability in the Santa Barbara Channel, *Aquat. Microb. Ecol., 20*, 129-145.

Pearson, P. N., B. E. van Dongen, C. J. Nicholas, R. D. Pancost, S. Schouten, J. M. Singano, and B. S. Wade (2007), Stable warm tropical climate through the Eocene Epoch, *Geology, 35*(3), 211-214.

Peterson, R. G., and L. Stramma (1991), Upper-Level Circulation in the South-Atlantic Ocean, *Prog. Oceanogr., 26*(1), 1-73.

Prahl, F. G., and S. G. Wakeham (1987), Calibration of unsaturation patterns in long-chain ketone compositions for paleotemperature assessment, *Nature, 330*, 367-369.

Prahl, F. G., G. J. de Lange, M. Lyle, and M. A. Sparrow (1989), Post-depositional stability of long chain alkenones under constrasting redox conditions, *Nature, 341*, 434-437.

Prahl, F. G., T. D. Herbert, S. C. Brassell, N. Ohkouchi, M. Pagani, D. J. Repeta, A. Rosell-Melé, and E. L. Sikes (2000), Status of alkenone paleothermometer calibration: Report from Working Group 3, *G3 (Geochem., Geophys., Geosyst.)*, (1), doi: Paper number 2000GC000058.

Reid, J. L. (1989), On the Total Geostrophic Circulation of the South-Atlantic Ocean - Flow Patterns, Tracers, and Transports, *Prog. Oceanogr., 23*(3), 149-244.

Robert, C., L. Diester-Haass, and J. Paturel (2005), Clay mineral assemblages, siliciclastic input and paleoproductivity at ODP Site 1085 off Southwest Africa: A late Miocene-early Pliocene history of Orange river discharges and Benguela current activity, and their relation to global sea level change, *Mar. Geol., 216*(4), 221-238.

Rontani, J. F., P. Bonin, I. Jameson, and J. K. Volkman (2005), Degradation of alkenones and related compounds during oxic and anoxic incubation of the marine haptophyte Emiliania huxleyi with bacterial consortia isolated from microbial mats from the Camargue, France, *Org. Geochem., 36*(4), 603-618.

Rontani, J. F., R. Harji, S. Guasco, F. G. Prahl, J. K. Volkman, N. B. Bhosle, and P. Bonin (2008), Degradation of alkenones by aerobic heterotrophic bacteria: Selective or not?, *Org. Geochem., 39*(1), 34-51.

Roters, B., and R. Henrich (2010), The middle to late Miocene climatic development of Southwest Africa derived from the sedimentological record of ODP Site 1085A, *Int. J. Earth Sci.*, *99*(2), 459-471.

Roveri, M., S. Lugli, V. Manzi, and B. C. Schreiber (2008), The Messinian Sicilian stratigraphy revisited: new insights for the Messinian salinity crisis, *Terra Nova*, *20*(6), 483-488.

Rühlemann, C., S. Mulitza, G. Lohmann, A. Paul, M. Prange, and G. Wefer (2004), Intermediate depth warming in the tropical Atlantic related to weakened thermohaline circulation: Combining paleoclimate data and modeling results for the last deglaciation, *Paleoceanography*, *19*(1), -.

Schleper, C., and G. W. Nicol (2010), Ammonia-Oxidising Archaea – Physiology, Ecology and Evolution *Adv. Microb. Pysiol.*, *57*, 1-41.

Schneider, B., and A. Schmittner (2006), Simulating the impact of the Panamanian seaway closure on ocean circulation, marine productivity and nutrient cycling, *Earth Planet. Sci. Lett.*, *246*(3-4), 367-380.

Schneider, R. R., et al. (2003), *Report and priliminary results of METEOR Cruise M 57/1, Cape Town - Walvis Bay, 20.01. - 08.02.2003*, 123 pp., Universität Bremen, Germany, Bremen.

Schouten, S., E. C. Hopmans, and J. S. S. Damste (2004), The effect of maturity and depositional redox conditions on archaeal tetraether lipid palaeothermometry, *Org. Geochem.*, *35*(5), 567-571.

Schouten, S., E. C. Hopmans, E. Schefuß, and J. S. Sinninghe Damsté (2002), Distributional variations in marine crenarchaeotal membrane lipids: a new tool for reconstructing ancient sea water temperatures, *Earth Planet. Sci. Lett.*, *204*, 265-274.

Schouten, S., A. Forster, F. E. Panoto, and J. S. S. Damste (2007a), Towards calibration of the TEX86 palaeothermometer for tropical sea surface temperatures in ancient greenhouse worlds, *Org. Geochem.*, *38*(9), 1537-1546.

Schouten, S., C. Huguet, E. C. Hopmans, M. V. M. Kienhuis, and J. S. S. Damste (2007b), Analytical methodology for TEX86 paleothermometry by high-performance liquid chromatography/atmospheric pressure chemical ionization-mass spectrometry, *Anal. Chem.*, *79*(7), 2940-2944.

Schulz, H., and a. C. Participants (1992), Bericht und erste Ergebnisse über die Meteor-Fahrt M20/2, Abidjan–Dakar, 27.12.1991–3.2.1992., *Berichte, Fachbereich Geowissenschaften*, *25*.

Shah, S. R., G. Mollenhauer, N. Ohkouchi, T. I. Eglinton, and A. Pearson (2008), Origins of archaeal tetraether lipids in sediments: Insights from radiocarbon analysis, *Geochim. Cosmochim. Acta*, *72*(18), 4577-4594.

Shannon, L. V., and G. Nelson (1996), The Benguela: large scale features and processes and system variability, in *The South Atlantic: Present and Past Circulation*, edited by G. Wefer, W. H. Berger, G. Siedler and D. J. Webb, Springer-Verlag, Berlin.

Shevenell, A. E., J. P. Kennett, and D. W. Lea (2004), Middle Miocene Southern Ocean cooling and Antarctic cryosphere expansion, *Science*, *305*(5691), 1766-1770.

Siesser, W. G. (1980), Late Miocene Origin of the Benguela Upswelling System Off Northern Namibia, *Science*, *208*(4441), 283-285.

Sinninghe Damsté, J. S., S. Schouten, E. C. Hopmans, A. C. T. van Duin, and J. A. J. Geenevasen (2002), Crenarchaeol: the characteristic core glycerol dibiphytanyl glycerol tetraether membrane lipid of cosmopolitan pelagic crenarchaeota, *J. Lipid Res.*, *43*(10), 1641-1651.

Sluijs, A., et al. (2006), Subtropical arctic ocean temperatures during the Palaeocene/Eocene thermal maximum, *Nature*, *441*(7093), 610-613.

Stramma, L., and M. England (1999), On the water masses and mean circulation of the South Atlantic Ocean, *J. Geophys. Res.-Oceans*, *104*(C9), 20863-20883.

Summerhayes, C. P. D., D. Kroon, A. Rosell-Melé, R. W. Jordan, H.-J. Schrader, R. Hearn, J. Vilanueva, J. O. Grimalt, and G. Eglinton (1995), Variability in the Benguela Current upwelling system over the past 70,000 years, *Prog. Oceanogr.*, *35*, 207-251.

Teece, M. A., J. M. Getliff, J. W. Leftley, R. J. Parkes, and J. R. Maxwell (1998), Microbial degradation of the marine prymnesiophyte Emiliania huxleyi under oxic and anoxic conditions as a model for early diagenesis: long chain alkadienes, alkenones and alkyl alkenoates, *Org. Geochem.*, *29*(4), 863-880.

Thierstein, H. R., K. R. Geitzenauer, and B. Molfino (1977), Global Synchroneity of Late Quaternary Coccolith Datum Levels - Validation by Oxygen Isotopes, *Geology*, *5*(7), 400-404.

van Assen, E., K. F. Kuiper, N. Barhoun, W. Krijgsman, and F. J. Sierro (2006), Messinian astrochronology of the Melilla Basin: Stepwise restriction of the Mediterranean-Atlantic connection through Morocco, *Palaeogeogr. Palaeoclimatol. Palaeoecol.*, *238*(1-4), 15-31.

van Bennekom, A. J., and G. W. Berger (1984), Hydrography and Silica Budget of the Angola Basin, *Neth. J. Sea Res.*, *17*(2-4), 149-200.

Vellinga, M., and R. A. Wood (2002), Global climatic impacts of a collapse of the Atlantic thermohaline circulation, *Clim. Change*, *54*(3), 251-267.

Vidal, L., T. Bickert, G. Wefer, and U. Rohl (2002), Late miocene stable isotope stratigraphy of SE Atlantic ODP Site 1085: Relation to Messinian events, *Mar. Geol.*, *180*(1-4), 71-85.

Villanueva, J., J. A. Flores, and J. O. Grimalt (2002), A detailed comparison of the U-37(k ') and coccolith records over the past 290 years: implications to the alkenone paleotemperature method, *Org. Geochem.*, *33*(8), 897-905.

Wefer, G., W. H. Berger, G. Siedler, and D. J. Webb (1996), *The South Atlantic*, Springer, Berlin.

Wefer, G., W. H. Berger, C. Richter, and S. S. P. ODP (1998), *Proc. Ocean Drill. Program: Initial Rep.*, 577 pp., College Station, TX.

Weigelt, E., and G. Uenzelmann-Neben (2004), Sediment deposits in the Cape Basin: Indications for shifting ocean currents?, *Aapg Bull.*, *88*(6), 765-780.

Weijers, J. W. H., S. Schouten, O. C. Spaargaren, and J. S. S. Damste (2006), Occurrence and distribution of tetraether membrane lipids in soils: Implications for the use of the TEX86 proxy and the BIT index, *Org. Geochem.*, *37*(12), 1680-1693.

Weijers, J. W. H., S. Schouten, J. C. van den Donker, E. C. Hopmans, and J. S. S. Damste (2007), Environmental controls on bacterial tetraether membrane lipid distribution in soils, *Geochim. Cosmochim. Acta*, *71*(3), 703-713.

Westerhold, T., T. Bickert, and U. Rohl (2005), Middle to late Miocene oxygen isotope stratigraphy of ODP site 1085 (SE Atlantic): new constrains on miocene climate variability and sea-level fluctuations, *Palaeogeogr. Palaeoclimatol. Palaeoecol.*, *217*(3-4), 205-222.

Williams, M., A. M. Haywood, S. P. Taylor, P. J. Valdes, B. W. Sellwood, and C. D. Hillenbrand (2005), Evaluating the efficacy of planktonic foraminifer calcite $\delta^{18}O$ data for sea surface temperature reconstruction for the Late Miocene, *Geobios*, *38*(6), 843-863.

Woodruff, F., and S. M. Savin (1989), Miocene deepwater oceanography, *Paleoceanography*, *4*, 87-140.

Wuchter, C., S. Schouten, M. J. L. Coolen, and J. S. Sinninghe Damsté (2004), Temperature-dependent variation in the distribution of tetraether membrane lipids of marine Crenarchaeota: Implications for TEX_{86} paleothermometry, *Paleoceanography*, *19*.

Wuchter, C., S. Schouten, S. G. Wakeham, and J. S. S. Damste (2005), Temporal and spatial variation in tetraether membrane lipids of marine Crenarchaeota in particulate organic matter: Implications for TEX86 paleothermometry, *Paleoceanography*, *20*(3), -.

Wuchter, C., et al. (2006), Archaeal nitrification in the ocean, *Proc. Natl. Acad. Sci. U. S. A.*, *103*(33), 12317-12322.

Zachos, J., M. Pagani, L. Sloan, E. Thomas, and K. Billups (2001), Trends, rhythms, and aberrations in global climate 65 Ma to present, *Science*, *292*(5517), 686-693.

9. Figure captions

Figure 1

Partial map of Africa showing the bathymetry of the Southeast Atlantic Ocean, position of ODP Site 1084 and 1085, major wind directions (dashed arrows) as well as major upper geostrophic oceanic currents (grey arrows) and basins [after *Leroux*, 1983; *van Bennekom and Berger*, 1984]. The Benguela Current comprises two components, the inner Benguela Coastal Current (BCC) and the outer Benguela Oceanic Current (BOC). Both flow northward over the Walvis Ridge. Shading identifies areas of modern perennial upwelling and upwelling filaments [after *Lutjeharms and Meeuwis*, 1987; *Lutjeharms and Stockton*, 1987]. The Orange River and its tributaries on the southern African continent are depicted. The dashed line represents the N-S transect of the rough sketch of modern East Atlantic water mass distribution showing different water masses (inset). The hydrographic scheme of the Southeast Atlantic is based on inorganic $\delta^{13}C$ data of GEOSECS and *Kroopnick* [1985] and on South Atlantic hydrography of *Stramma and England* [1999] and *Gersonde et al.* [1999]. The black arrows indicate the major flow directions of deep currents connected to the global conveyor belt.

Figure 2

Data from ODP core 1085A (Leg 175) between 13.7 and 2.8 Ma. A: $\delta^{18}O$ values of benthic foraminifera (a combined dataset of *Diester-Haass et al.* [2004], *Vidal et al.* [2002] and *Westerhold et al.* [2005]) with 20-point moving average (black line). B: water temperature data estimated using the alkenone based $U^{K'}_{37}$ index (open circles, white circles are data beyond calibration limit), calculated after *Müller et al.* [1998], and GDGT based TEX_{86} index (black dots, values with BIT > 0.3 printed in grey), calculated after *Kim et al.* [2010]. Error bars represent standard deviation of duplicate measurements. Implemented are SST_{UK} data from ODP Site 1084 (grey line; cf. Figure 1) adopted from *Marlow et al.* [2000], recalculated after *Müller et al.* [1998]. Light and dark grey areas correspond to the errors of the temperature calibration equations for SST_{UK} (±1°C [*Müller et al.*, 1998]) and $Temp_{TEX}$ (±2.5°C [*Kim et al.*, 2010]), respectively. C: ΔTemp calculated by subtraction of $Temp_{TEX}$ from SST_{UK}, displayed are ΔTemp values of reliable temperature estimations. Error bars represent propagated analytical errors. The upper and lower lines represent propagated errors

of calibration equations for the temperature proxies. D: TOC contents adapted from *Diester-Haass et al.* [2004] (grey line) and from this study (black dots). See text for more details. Abbreviations and explanations: $\delta^{18}O$, (‰ vs. V-PDB); SST, sea surface temperature (°C); TOC, total organic carbon content percentages.

Figure 3

a) Sea surface temperature estimates derived from SST_{UK} (grey dots and trend line) and $Temp_{TEX}$ (black dots and trend line) of a study of core top sediments within the upwelling area of the Cape Basin as well as satellite-derived SSTs for individual core top sites (crosses and dashed trend line) *versus* water depth in meter below sea surface. All data are adapted from *Lee et al.* [2008]. b) TOC values from a study of *Inthorn et al.* [2006] of the same core top sediments as used for Figure 3a are plotted against ΔTemp calculated by subtraction of $Temp_{TEX}$ data from SST_{UK} data from *Lee et al.* [2008]. Black dots refer to sites within perennial upwelling, grey dots represent sites at a water depth of 600 to 2000 m at the continental slope, open circles denote sites at a water depth of >2000 m being furthest away from the coast.

Table 1 showing log depth after *Wefer et al.* [1998], age after *Berger et al.* [2002], *Vidal et al.* [2002] and *Westerhold et al.* [2005], total organic carbon, BIT, standard deviation (S.D.) of BIT data, water temperatures calculated by $U^{K'}_{37}$ and TEX_{86} index, and standard deviation for $Temp_{TEX}$ data of samples from ODP Site 1085 A.

Log depth [mcd]	Age [Ma]	TOC [%]	BIT	S.D. BIT	$U^{K'}_{37}$	S.D. $U^{K'}_{37}$	SST_{UK} [°C]	S.D. SST_{UK} [°C]	TEX_{86}	S.D. TEX_{86}	$Temp_{TEX}$ [°C]	S.D. $Temp_{TEX}$ [°C]
0.7	0.015	1.23	0.07	0.00	0.64	0.00	18.0	0.1	0.53	0.02	19.7	1.3
1.3	0.032	1.29	0.15	0.12	0.59	0.01	16.6	0.2	0.46	0.01	15.8	0.8
2.6	0.069	1.23	0.08	0.01	0.64	0.00	18.1	0.1	0.54	0.03	20.2	1.5
134.8	2.849	1.04	0.08	0.00	0.69	0.00	19.5	0.1	0.50	0.03	15.8	1.9
135.5	2.861	1.45	0.09	0.01	0.68	0.01	19.1	0.3	0.46	0.02	15.1	1.1
138.6	2.905	1.78	0.08	0.00	0.64	0.00	18.1	0.1	0.50	0.01	15.9	0.5
148.3	3.064	1.55	0.10	0.00	0.68	0.01	19.3	0.2	0.48	0.01	14.4	0.4
160.6	3.267	1.19	0.11	0.00	0.72	0.01	20.6	0.3	0.47	0.00	16.4	0.0
165.7	3.352	0.96	0.07	0.00	0.71	0.01	20.1	0.2	0.50	0.02	15.5	1.5
176.9	3.546	1.42	0.13	0.00	0.69	-	19.6	-	0.60	0.00	16.2	0.1
190.9	3.787	1.24	0.15	0.00	0.68	0.01	19.3	0.3	0.49	0.03	16.5	1.6
197.4	3.896	1.06	0.12	0.00	0.76	0.00	21.7	0.1	0.48	0.00	18.3	0.0
205.6	4.020	0.86	0.18	0.01	0.72	0.00	20.5	0.1	0.65	0.01	15.3	0.4
227.3	4.315	1.15	0.12	0.00	0.77	0.01	22.0	0.2	0.49	0.00	18.9	0.1
232.4	4.381	0.76	0.08	0.00	0.72	0.01	20.5	0.2	0.52	0.00	17.5	0.3
239.5	4.477	0.71	0.15	0.00	0.73	0.01	20.7	0.3	0.52	0.00	17.9	0.1
247.6	4.587	1.03	0.13	0.00	0.74	0.01	21.0	0.2	0.57	0.01	17.4	0.7
255.8	4.731	1.52	0.16	0.00	0.73	0.00	20.8	0.1	0.54	0.00	17.2	0.2
261.9	4.943	1.21	0.11	0.00	0.71	0.00	20.2	0.1	0.53	0.00	16.7	0.3
269.1	5.086	0.73	0.13	0.01	0.75	0.01	21.5	0.2	0.51	0.01	19.3	0.7
281.4	5.249	0.98	0.20	0.00	0.78	0.01	22.4	0.3	0.62	0.03	24.2	1.4
303.4	5.529	1.02	0.06	0.01	0.76	0.04	21.6	1.3	0.68	0.07	25.0	-
331.2	5.971	1.07	0.03	0.03	0.66	0.03	18.5	1.1	0.50	0.03	18.2	1.9
352.2	6.277	0.76	0.24	0.01	0.74	0.00	21.1	0.1	0.60	0.04	23.6	2.1
359.8	6.471	0.78	0.15	0.00	0.74	0.00	21.2	0.1	0.55	0.00	20.7	0.1

360.1	6.486	0.61	0.16	0.00	0.74	0.01	21.0	0.2	0.53	0.04	19.6	2.4
360.4	6.510	0.49	0.14	-	0.76	0.00	21.8	0.0	0.54	-	20.3	-
365.8	6.764	0.47	0.04	0.01	0.75	0.03	21.3	1.0	0.50	0.01	18.0	0.3
366.8	6.812	0.30	0.07	0.03	0.73	0.04	20.8	1.2	0.53	0.04	19.7	2.4
371.2	6.967	0.47	0.20	0.01	0.79	0.00	22.5	0.1	0.55	0.00	21.0	0.2
371.6	6.986	0.50	0.18	0.00	0.77	0.00	22.0	0.0	0.56	0.02	21.1	0.8
371.9	7.001	0.66	0.18	0.01	0.76	0.00	21.6	0.0	0.52	0.01	19.1	0.8
384.3	7.408	0.62	0.09	0.01	0.79	0.00	22.5	0.2	0.52	0.00	19.3	0.0
393.9	7.594	0.62	0.11	0.01	0.78	0.01	22.5	0.1	0.53	0.00	19.7	0.1
404.4	7.813	0.69	0.08	0.03	0.84	0.01	24.2	0.1	0.54	0.00	20.2	0.0
414.0	8.232	0.66	0.09	0.01	0.80	0.01	22.8	0.3	0.53	0.03	19.6	1.8
423.7	8.613	0.49	0.06	0.01	0.83	0.03	23.8	1.1	0.55	0.01	20.7	0.3
427.9	8.787	0.64	0.07	0.01	0.81	0.02	23.3	0.8	0.53	0.01	19.5	0.4
433.3	9.019	0.63	0.20	0.00	0.86	0.01	24.8	0.2	0.57	0.01	21.7	0.5
433.8	9.032	0.78	0.16	0.01	0.82	0.01	23.6	0.4	0.53	0.03	19.7	1.9
434.2	9.042	0.79	0.19	0.01	0.84	0.01	24.1	0.4	0.52	0.01	19.1	0.5
445.4	9.386	0.63	0.08	0.01	0.88	-	25.2	-	0.50	0.00	17.9	0.0
451.0	9.582	0.72	0.10	0.04	0.83	0.03	23.9	0.8	0.57	0.00	21.7	0.2
467.0	10.033	0.55	0.17	0.02	0.88	0.00	25.5	0.0	0.57	0.01	21.9	0.4
467.1	10.041	0.69	0.18	0.00	0.88	0.02	25.4	0.6	0.54	0.02	20.2	1.3
467.3	10.051	0.55	0.19	0.01	0.87	0.00	25.1	0.1	0.57	0.00	21.9	0.2
481.0	10.422	0.62	0.09	0.01	0.87	-	24.9	-	0.56	0.02	21.6	1.2
489.8	10.553	0.53	0.31	0.01	0.87	-	25.0	-	0.64	0.04	25.1	2.1
499.8	10.703	0.53	0.13	0.06	0.90	-	25.8	-	0.61	0.06	23.8	2.9
518.6	10.984	0.34	0.19	0.00	0.92	0.00	26.5	0.1	0.61	0.02	23.7	0.8
518.8	10.987	0.33	0.24	0.00	0.90	0.00	26.0	0.2	0.60	0.00	23.7	0.2
519.3	10.994	0.34	0.23	0.02	0.89	0.00	25.7	0.2	0.60	0.01	23.4	0.3
537.4	11.369	0.20	0.57	0.04	0.91	-	26.2	-	0.71	0.02	28.6	0.9
550.5	11.627	0.26	0.16	0.01	0.93	0.02	26.8	0.5	0.64	0.01	25.2	0.2
558.4	11.957	0.20	0.49	0.04	0.95	-	27.5	-	0.70	0.01	28.1	0.5

562.4	12.118	0.22	0.64	0.13	0.94	-	27.2	-	0.67	-	26.9	-
568.1	12.422	0.35	0.45	0.02	0.94	0.00	27.1	0.1	0.70	0.00	28.1	0.2
573.0	12.622	0.24	0.71	0.06	0.93	-	26.9	-	0.69	-	27.8	-
576.9	12.827	0.16	0.62	0.09	0.92	-	26.4	-	0.73	-	29.2	-
579.5	12.945	0.19	0.69	0.00	0.91	-	26.3	-	0.75	0.04	29.9	1.6
579.7	12.957	0.18	0.75	0.00	0.91	-	26.2	-	0.72	0.04	28.8	1.5
579.9	12.969	0.14	0.75	0.00	0.90	-	26.0	-	0.76	0.04	30.5	1.5
581.4	13.064	0.32	0.48	0.09	0.91	0.01	26.2	0.2	0.68	0.06	27.3	2.6
585.3	13.344	0.11	0.88	0.02	0.91	-	26.1	-	0.74	0.01	29.7	0.5
588.4	13.547	0.11	0.66	0.04	0.94	-	27.2	-	0.76	-	30.5	-
591.3	13.708	0.13	0.71	0.12	0.94	-	27.0	-	0.75	-	30.0	-

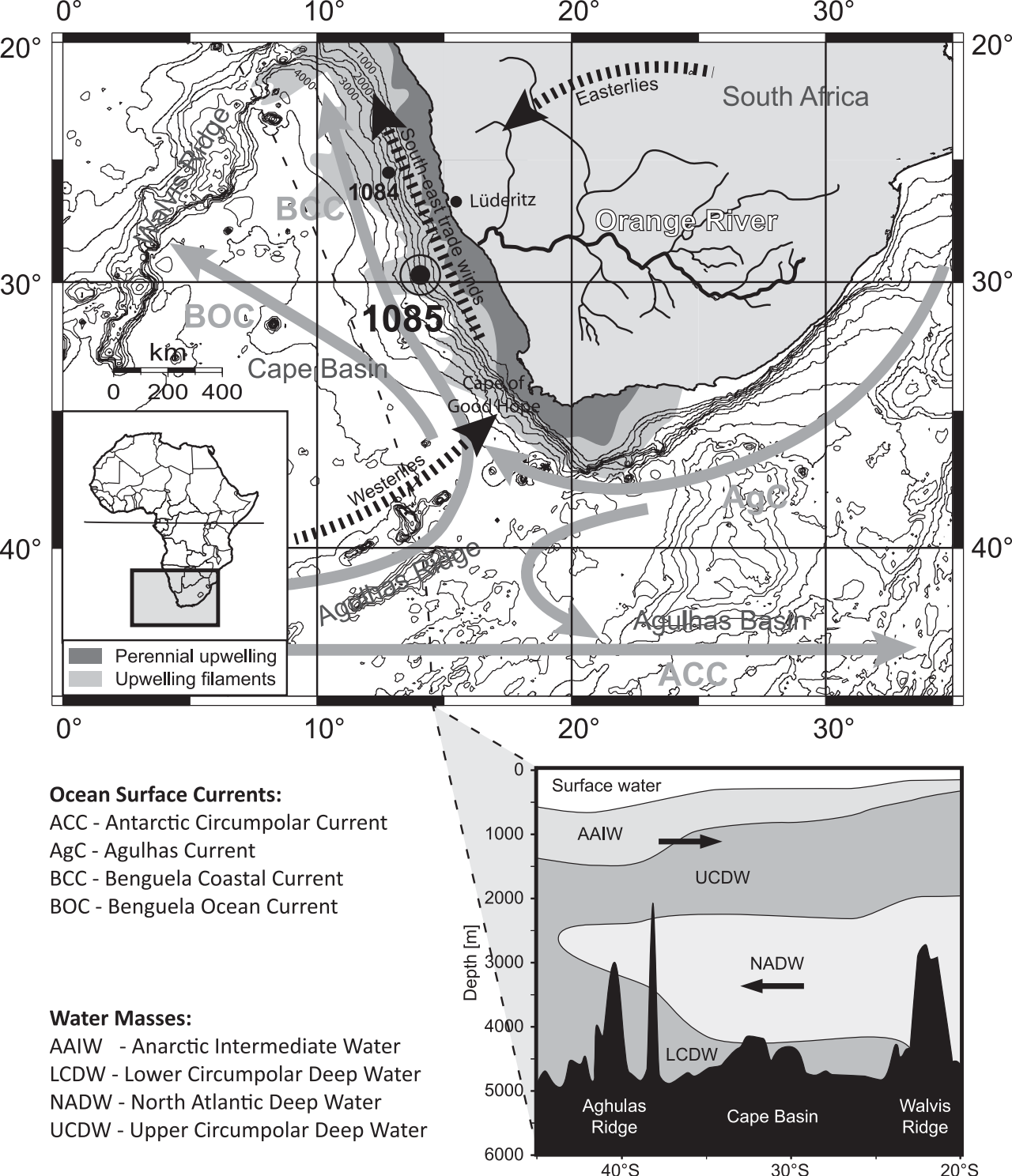

Ocean Surface Currents:

ACC - Antarctic Circumpolar Current
AgC - Agulhas Current
BCC - Benguela Coastal Current
BOC - Benguela Ocean Current

Water Masses:

AAIW - Anarctic Intermediate Water
LCDW - Lower Circumpolar Deep Water
NADW - North Atlantic Deep Water
UCDW - Upper Circumpolar Deep Water

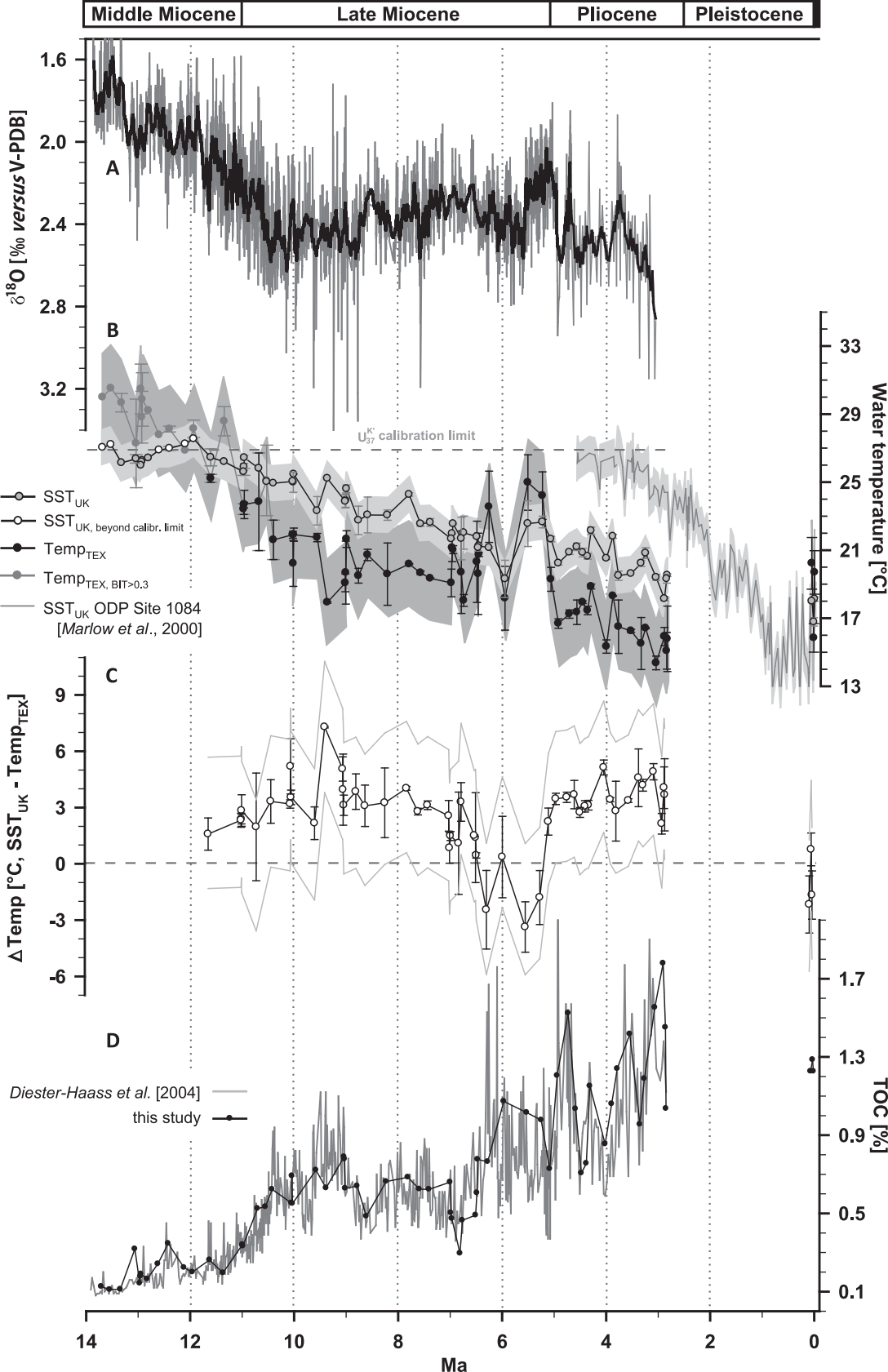
Middle Miocene
Late Miocene
Pliocene
Pleistocene
A
B
C
D
δ18O [‰ versus V-PDB]
Water temperature [°C]
ΔTemp [°C, SSTUK - TempTEX]
TOC [%]
Ma
U37K' calibration limit
SSTUK
SSTUK, beyond calibr. limit
TempTEX
TempTEX, BIT>0.3
SSTUK ODP Site 1084
[Marlow et al., 2000]
Diester-Haass et al. [2004]
this study

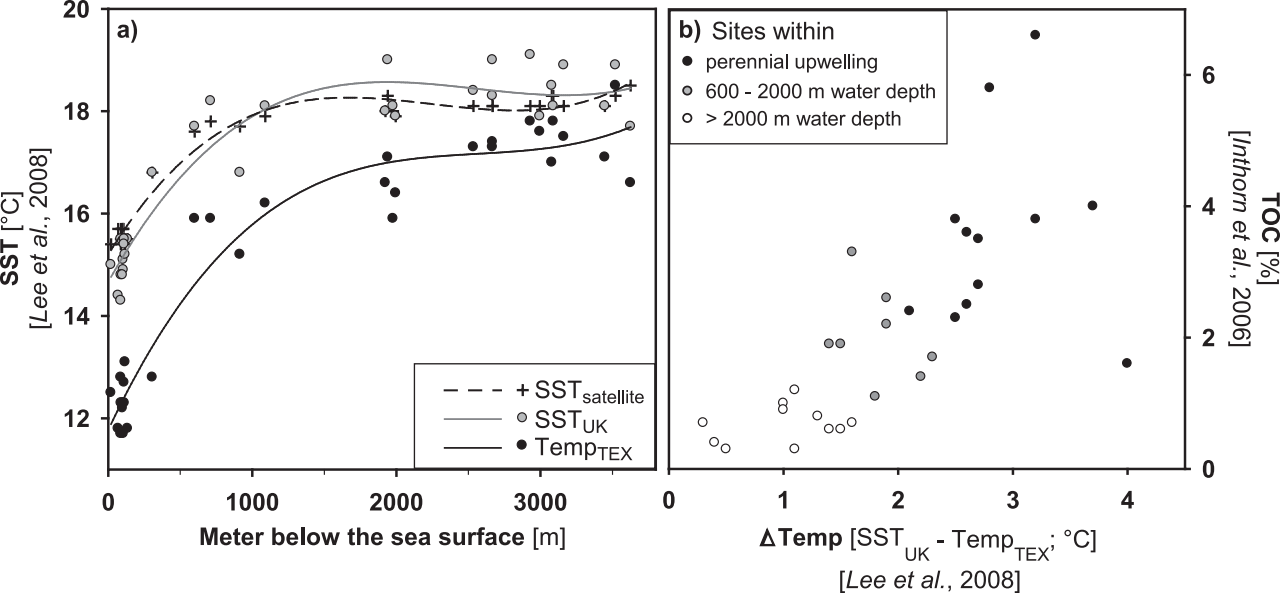
a)
b) Sites within
perennial upwelling
600 - 2000 m water depth
> 2000 m water depth
SST [°C]
[Lee et al., 2008]
TOC [%]
[Inthorn et al., 2006]
+ SST satellite
SST UK
Temp TEX
Meter below the sea surface [m]
ΔTemp [SST UK - Temp TEX; °C]
[Lee et al., 2008]
20
18
16
14
12
0
1000
2000
3000
1
2
3
4
6
4
2
0